Phase field simulation study of the attachment of metallic droplets to solid particles in liquid slags based on real slag-spinel micrographs

Inge Bellemans[a], Evelien De Wilde[a], Nele Moelans[b], Kim Verbeken[a]

[a] Department of Materials Science and Engineering, Ghent University, Technologiepark 903, B-9052 Zwijnaarde (Ghent), Belgium: inge.bellemans@ugent.be (+32 9 3310441), evelien.dewilde@ugent.be (+32 9 3310447), kim.verbeken@ugent.be (+32 9 3310453)

[b] Department of Materials Engineering, KU Leuven, Kasteelpark Arenberg 44 (box 2450), B-3001 Leuven, Belgium: Nele.Moelans@mtm.kuleuven.be (+32 16 321316)

Abstract

Pyrometallurgical industries encounter production losses due to the attachment of metallic droplets to solid particles in liquid slags. Experimental work on this topic remains very challenging. Simulations based on a phase field model can circumvent this lack of experimental data and allow a more systematic insight into the role of the different parameters on the observed phenomenon.

In the present work, a recently developed phase-field model to simulate the attachment of liquid metal droplets to solid particles in slags is extended to consider real microstructures of solid particles in liquid slags. Furthermore, it is investigated which initialization method for the liquid metal droplets corresponds best to the experimental conditions. One of the initialization methods used spinodal decomposition of a supersaturated slag to introduce the metallic droplets, whereas the other initialization consists of positioning metallic droplets in the slag in a random way. The simulations showed that both initialization methods result in microstructures that correspond with experimental observations, which points to the existence of several origins for the attachment of metal droplets to solid particles in slags.

Keywords

Phase field model; Droplets; Spinodal decomposition; Random initialization method

1 Introduction

Phase separation at the end of pyrometallurgical operations is usually obtained by the introduction of a sedimentation step. Unfortunately, the slag and matte/metal phase are not perfectly separated during sedimentation and valuable metals are lost in the slag or reprocessing of this phase is required. The loss of metal/matte droplets can be caused by various sources, of which the attachment to solid particles in the liquid slag phase [1] is the least investigated. This attachment is responsible for production losses in industrial Cu smelters [2,3], Pb reduction melting furnaces [4] and other industries [5].

To understand the fundamental nature of the interaction, experimental efforts were reported recently [1,6,7]. The first experiments pointed towards an important role of interfacial energies in this interaction. As modelling can help to study the interaction between the solid particles and metallic droplets, experiments and modelling were used in a complementary way. A previously developed phase field model [8,9] describes the growth and evolution of liquid metal droplets by spinodal decomposition in a liquid oxide phase (representing the slag) with dispersed solid oxide particles. In our previously reported modelling work [8,9], the influence of the interfacial energies on the attachment of metallic droplets to solid particles was investigated and four different wetting regimes were determined, namely no wettability of the metal on the particle, low wettability, high wettability and full wettability. [8] Moreover, the model was used to investigate the influence of the particle morphology on the behaviour of the liquid metal droplets in different wetting regimes. In addition, the simulations were used to classify and interpret experimental observations in a synthetic, but industrially relevant PbO-

FeO-CaO-SiO_2-Cu_2O-ZnO-Al_2O_3 system [1]. E.g. it was observed that one metallic droplet was often attached to several solid particles, as shown in Figure 1.

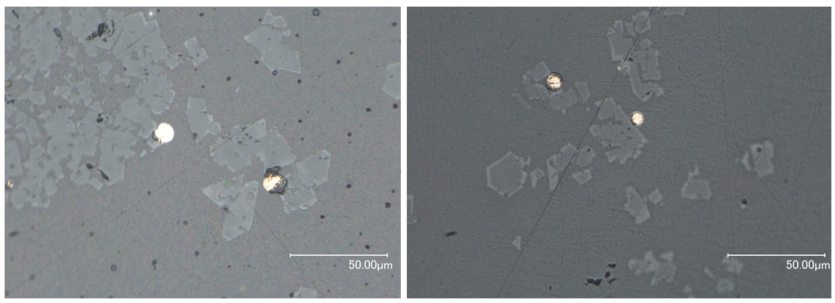

FIGURE 1 EXPERIMENTALLY OBTAINED MICROGRAPHS OF ONE CU DROPLET ATTACHED TO SEVERAL SPINEL PARTICLES. THESE OPTICAL MICROGRAPHS WERE OBTAINED FROM OPTICAL MICROSCOPY ON A QUENCHED SAMPLE AFTER SMELTING ALL COMPONENTS IN A PBO-FEO-CAO-SIO_2-CU_2O-ZNO-AL_2O_3 SYSTEM AT 1200°C [1]

Comparison of the simulations with the experiments in previous work [9] indicated that the experimental system corresponds best to the low wettability case. Moreover, the Cu droplets in the experimentally obtained micrographs, such as in Figure 1, have a quasi-spherical shape and a large contact angle, also indicating a good correspondence to the low wettability regime.

In this paper, the existing phase field model is extended to consider realistic microstructures based on actual micrographs of the slag with solid spinel particles and the origin of the attachment is investigated in more detail by comparing simulations using two different initialization methods for the metal droplets. The model is first summarized in section 2, the reader is referred to [8] for more information concerning this model. Section 3 considers the simulation set-up: the simulation parameters, the numerical implementation, the extension of the model and the initialization methods. Finally, the results are presented and discussed in section 4.

2 Model formulation

2.1 Variables and free energy functional

A hypothetical binary system O-M is considered and the model should describe a microstructure with a solid phase and two liquid phases that differ in composition, i.e. a liquid metal and a liquid oxide. For this, a non-conserved phase-field variable ϕ was introduced to distinguish between the solid ($\phi = 1$) and the liquid phases ($\phi = 0$). Moreover, to be able to distinguish the liquid phases, a conserved composition field x_M describes the local molar fraction of the metallic element. Figure 2 illustrates the correspondence between the experimental and simulated situations.

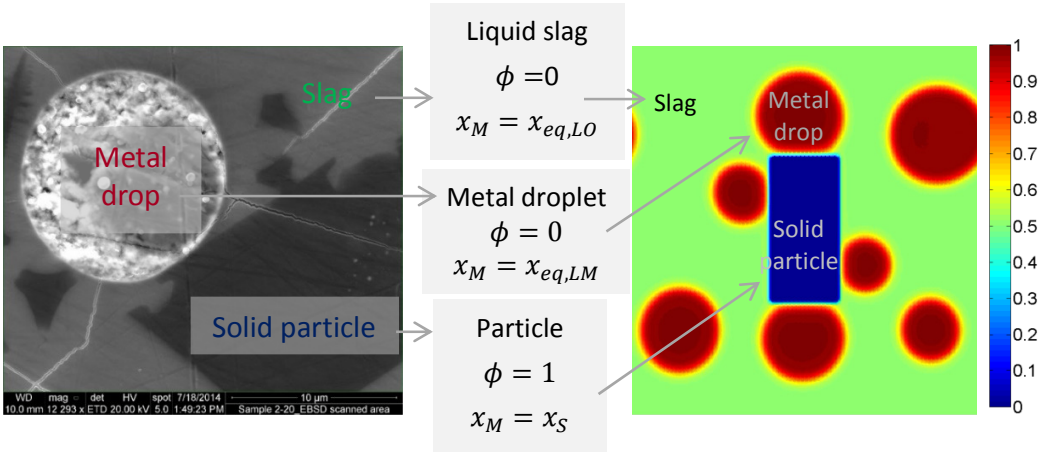

FIGURE 2 ILLUSTRATION OF HOW THE VALUE OF THE FIELD VARIABLES (x_M - Φ x_S) IN THE SIMULATIONS (ON THE RIGHT) CORRESPOND TO THE EXPERIMENTAL SITUATION (LEFT)

Here, $x_{eq,LO}$ and $x_{eq,LM}$ are the equilibrium compositions of the oxidic liquid (slag), indicated with 'LO', and of the metallic liquid, indicated with 'LM', respectively. x_S determines the equilibrium composition of the solid particle. This particle is assumed to not react with the liquid phases and thus its composition remains constant.

Both field variables (ϕ and x_M) are continuous functions in space and time. The position of the boundaries between different phases is implicitly given by the value of these field variables, i.e. they change continuously from one bulk value to another bulk value over the interface, representing a diffuse interface, which is characteristic for the phase field method [10]. The

temperature and pressure of the system are assumed to be constant and the molar volume V_m is the same in all phases and is independent of composition. Convection is not considered. The solid particles are assumed to be present before droplet formation and their composition is fixed.

2.2 Evolution equations

The microstructural evolution in an isothermal system at constant pressure is driven by minimization of the total Gibbs energy. The evolution of the mole fraction of the metallic element is governed by the following mass balance equation

$$\frac{\partial x_M}{\partial t} = \nabla \cdot [\mathrm{M}\, \nabla \left[\left(1 - h(\phi)\right) f'_{Liquid}(x_M) + h(\phi) f'_{Solid}(x_M) - \kappa_{x_M} \nabla^2 x_M \right]] \qquad \textbf{(1)}$$

The coefficient M (m^5/ (J s)) is related to the interdiffusion coefficient D (m²/s) of the liquid as $D = A_{Sp} M . \kappa_{x_M}$ (J/m) is the gradient energy coefficient for the liquid-liquid interfaces. A_{Sp} (J/m³) is the curvature of the free energy curve.

The homogeneous part of the free energy of the liquid phase is represented by the fourth order polynomial $f_{Liquid}(x_M) = \frac{A_{Sp}}{2} \left(x_M - x_{eq,LO}\right)^2 \left(x_M - x_{eq,LM}\right)^2$. This polynomial corresponds to a miscibility gap where $x_{eq,LO}$ and $x_{eq,LM}$ correspond to the equilibrium compositions of the free energy curve of the liquid [8]. Analogously, the bulk contribution of the solid phase as a function of composition is represented by a parabolic Gibbs energy $f_{Solid}(x_M) = \frac{A_S}{2} (x_M - x_S)^2$, as is usual in phase field modelling for stoichiometric solid phases [11,12]. x_S and A_S (J/m³) are model parameters that determine the position of the minimum and the curvature of the parabola describing the free energy curve of the solid. The interpolation function $h(\phi)$ is one that is frequently used in solid-liquid systems [8,11] and has the form $h(\phi) = \phi^3(10 - 15\phi + 6\phi^2)$.

The non-conserved phase field variable ϕ evolves according to the following equation [13]

$$\frac{\partial \phi}{\partial t} = -L\frac{\delta F}{\delta \phi} = -L\left[W g'(\phi) + h'(\phi)\left(f_{Solid} - f_{Liquid}\right) - \kappa_\phi \nabla^2 \phi\right] \quad \textbf{(2)}$$

Where W (J/m³) is the depth of the double well function and κ_ϕ (J/m) the gradient energy coefficient for the solid-liquid interfaces. L is the kinetic coefficient related to the velocity at which atoms can hop over an interface.

3 Simulation set-up

3.1 Constant parameters

The same parameter values were used as in [8] and [9]. These parameters are linked with properties in the physical system and the values of these properties are chosen based on typical orders of magnitudes for these specific parameters. Some compromises were made to limit the computation time, as explained below for each parameter. Several values and descriptions of the model parameters are listed in Table 1.

Symbol	Description	Value(s)
N	System size	[256 256 1] grid points
Δx	Grid spacing	$(4/\sqrt{10})\ 10^{-7}$ m
Δt	Time step spacing	10^{-4} s
$x_{eq,LO}$	Oxidic equilibrium composition of free energy curve of spinodal decomposition	0.50
$x_{eq,LM}$	Metallic equilibrium composition of free energy curve of spinodal decomposition	0.98
A_{Sp}	Steepness of free energy curve of spinodal decomposition	$4\ 10^8$ J/m³
A_S	Steepness of free energy curve of solid	$20\ 10^8$ J/m³
W	Depth of the double well function	$15\ 10^6$ J/m³
κ_ϕ	Gradient energy coefficient for the solid-liquid interfaces	$(15/8)\ 10^6$ J/m
L	Kinetic coefficient for the evolution of ϕ	10^{-30} m³/(J s)
$L_{initial}$	Kinetic coefficient for the evolution of ϕ for the first 1000 time steps	10^{-7} m³/(J s)
κ_{x_M}	Gradient energy coefficient for the liquid-liquid interfaces	$6\ 10^{-6}$ J/m
M	Mobility coefficient of the metal	10^{-19} m⁵/(J s)

TABLE 1 VALUES AND DESCRIPTIONS OF SEVERAL CONSTANT PARAMETERS IN THE MODEL

To avoid compositional changes in the solid phase during the initial stage of the simulation, the free energy curve of the solid was made five times steeper than the curve of the liquid phase, which is shown in the values of A_S and A_{Sp}. $\gamma_{LO,LM}$ should be of the order of 1 N/m [14,15] and the interfaces should at least contain five grid points for a sufficient resolution of the diffuse transition at interfaces and to reproduce accurately the surface energies [16]. This results in the parameter values mentioned in Table 1 and yields the following values of interfacial energy and interfacial widths throughout all simulations: $l_{LO,LM}$ = 8.0687 grid points (or 1.02 nm), $\gamma_{LO,LM}$ = 0.9030 N/m and $l_{S,LO} = l_{S,LM}$ = 7.9057 grid points (or 1 nm). M is chosen in such a way that the diffusion coefficient $D = 4\ 10^{-11}$ m²/s.

The particle is assumed to not react in these simulations, requiring a very small value of the kinetic coefficient L, but a larger value of L is used during the first 1000 time steps, allowing the interface to become diffuse as the field variables have sharp steps at the interfaces in the beginning of a simulation. Thus two different L-values are tabulated in Table 1.

Previous results illustrate the existence of four different wettability regimes: no, low, high and full wetting [8]. These different regimes can be attained by changing the interfacial energy, as described by Young's equation

$$\gamma_{S,LO} = \gamma_{S,LM} + \gamma_{LO,LM} \cos\theta \qquad \textbf{(3)}$$

In this model, the solid particle is assumed to not react and thus its composition x_S remains constant. This composition can be used as a parameter to adapt the interfacial energy. The effect of the x_S-value on the solid-liquid interfacial energies and the contact angle was demonstrated in our previous work [8]. Non-wetting is characterized by a non-existing contact angle and is expected for $x_S \leq 0.57$, a low wettability corresponds to $90° \leq \theta \leq 180°$ and is found

for x_S between 0.58 and 0.74. High wettability corresponds to 0°≤ θ ≤ 90° or x_s between 0.74 and 0.90 and full wetting also has a non-existing contact angle or x_S-values higher than 0.9. As mentioned in the introduction, the experimental system corresponds best to a low wettability system. Therefore, a low wettability regime was investigated in this work. An x_S-value of 0.58 was chosen as it is the limit between the no and low wettability regimes, because the experiments showed that the attached droplets have an almost spherical shape. In addition x_S = 0.50 was used to investigate the 'no wettability' situation.

3.2 Numerical implementation

The evolution of the variables, as described by the kinetic equations, is calculated using the semi-implicit Fourier spectral method [17]. Matlab [18] was used for the calculations. Typical computation times on an Intel® Core™ i7-3610QM CPU @ 2.30GHz processor with 8Gb RAM ranged from 2h to 4h for a system size of [256 256 1] and a simulation time of 10^6 time steps.

3.3 Initialization

3.3.1 Real microstructure of a slag containing solid particles

Previous work [8,9] only considered particles with simplified geometries. These simple morphologies approximate the spinel structure, which was observed for the solid particles to which the droplets attach in experiments. Previous simulations, however, also showed that the particle shape and distribution affect the amount of attached metal. Therefore, in this work the microstructure of the solid particles considered in the simulations was constructed based on actual experimental micrographs of these solid particles. In order to do this, the micrographs in the left hand side of Figure 3 were used as input for the 'imread' command in Matlab, turning every pixel of the photograph into a greyscale value. The micrographs are named photo 1 – 4 starting in the upper left corner to the lower right corner.

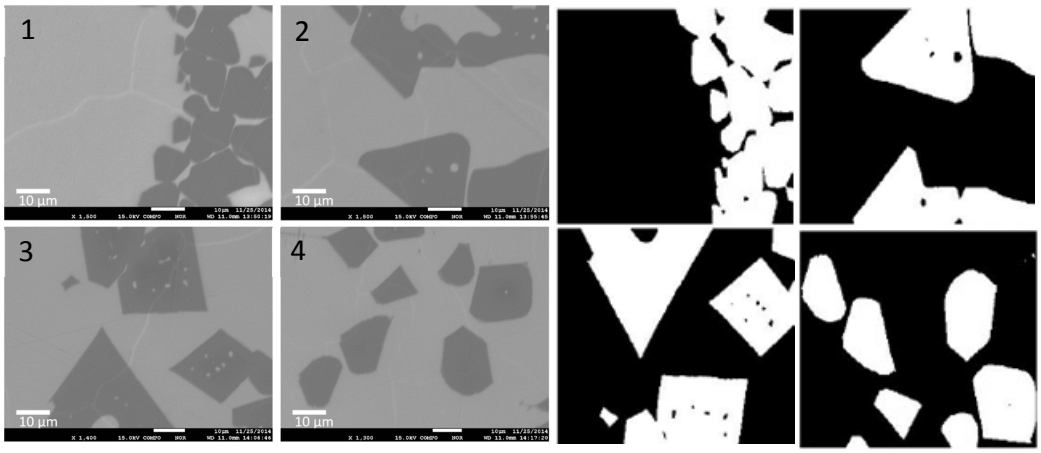

FIGURE 3 LEFT: SEM MICROGRAPH OF EXPERIMENTALLY OBTAINED MICROSTRUCTURE OF SOLID OXIDE PARTICLES IN A SLAG THAT WAS QUENCHED TO 'FREEZE' ITS HIGH TEMPERATURE CONDITION [1]; RIGHT: BLACK-AND-WHITE PICTURES THAT WERE USED AS INITIALIZATION FOR THE SOLID PARTICLES (WHITE: $\phi = 1$) WITHIN A LIQUID PHASE (BLACK: $\phi = 0$)

The edge with SEM information is then cut off, the pixels with a greyscale value above a certain threshold are treated as solid phase ($\phi = 1$) and the array containing these zeros and ones is then rescaled to the system size *N* in each dimension. The threshold value to which the greyscale values are compared is obtained by trial-and-error and can depend on the type of micrographs and the settings used to obtain them. For these SEM micrographs, a threshold value of 140 gave good results. This yielded the black-and-white figures in the right hand side of Figure 3, where white represents the solid ($\phi = 1$) and black the liquid ($\phi = 0$).

The corresponding particle fractions (defined by the area of all particles divided by the total system size, which is 65536 grid points for all cases) are tabulated in Table 2.

Photo	A = X*Y [grid points]	Particle density
1	19964	0.305
2	23989	0.366
3	26868	0.410
4	18646	0.285

TABLE 2 THE CALCULATED PARTICLE FRACTIONS FOR EVERY PHOTOGRAPH

In reality, large variations are found (from 2-6 wt% [19] to 25 wt% [6]) in the particle fraction and the conditions of the slag production play a very important role in this value. These values,

however, are averages over the complete slag phase and we are explicitly interested in regions with more solid particles. These regions were therefore considered in more detail in the experimentally obtained micrographs in Figure 3 and thus the simulations also deal with larger particle densities than the values averaged over the complete slag phase.

3.3.2 Comparison of two initialization methods for the metal droplets

The exact mechanism behind the interaction between the solid particles and liquid metal is not known. It is also not understood how and where the metal droplets originate. We compared two methods to initialize the metal droplets in the simulations: by spinodal decomposition of a supersaturated liquid (from now onward called 'spinodal initialization') and by a random positioning of droplets within the liquid phase (from now onward called 'random initialization'). The first would correspond in practice to a case where the droplets are formed by a reaction in which both the droplets and the spinel solids are involved. The latter corresponds to a situation where the droplets and particles are formed separately and independently and are then mixed in the slag. In both methods, the solid particles within the liquid slag are initialised by setting the value of ϕ equal to 1 and x_M equal to x_S within the areas corresponding to the solid particles in the original micrographs. The remaining liquid phase has a value of ϕ equal to 0.

The spinodal initialization provides an easy way to introduce the metals in the system. For decomposition into a liquid metal ($x_M = x_{eq,LM} = 0.98$) and a liquid oxide ($x_M = x_{eq,LO} = 0.50$), the uniform initial saturation of the solution x_i should be chosen between the inflection points of the spinodal liquid curve (where $\frac{\partial^2 G}{\partial x_M^2} < 0$) [20], namely: $0.601 < x_i < 0.879$. To initiate the spinodal decomposition, random noise is added, from a normal distribution with mean 0 and standard deviation 0.001, in every 100th time step. Industrial metal fractions in slags after

sedimentation are of the order of 5%. According to the lever rule, the minimal achievable value of the metal fraction in this model system is 0.211. Therefore, the x_i-values were kept minimal, but within the spinodal region. Furthermore, for $x_i > 0.66$, metal strands are formed instead of droplets in the model system. Therefore, an x_i value of 0.605 was chosen for the simulations, which corresponds to a volume fraction of metal of 0.219.

The alternative initialization method with 'random initialization' consists of randomly positioning droplets with a radius chosen from a discrete uniform random distribution between 1 and 10 times Δx in the system until the proposed volume fraction of metallic droplets is reached or slightly exceeded. Before the droplets are finally positioned within the system, it is checked that no overlap is present with the solid phase or other droplets already present in the system. Whenever this is the case, another position is looked for within the system. If no appropriate position is found after 20 trials, the initialization is aborted and the simulation is started with the droplets positioned in the system until then. The droplets are immediately initialized with their equilibrium composition of 0.98 ($x_{eq,LM}$) and the slag in between the droplets is initialised with a composition of 0.50 ($x_{eq,LO}$). The volume fraction of metal droplets was 0.20, corresponding to x_i-values of 0.596, which is close to the value of x_i used for spinodal decomposition, thus enabling us to compare both methods. The random noise term is not included in the simulations with random initialization.

3.4 Post-processing

A metal droplet is defined as the connected domain where $x_M - \phi x_S$ is larger than 0.71 and the particle where $0.5 < \phi$. A droplet was assigned to be 'attached' to the particle when overlap occurred between the with 2 grid point layers enlarged droplet and the particle which was

enlarged with 3 grid point layers. The fraction of attached metal is defined as the ratio of the total area of the attached droplets to the total area of metal droplets in the system. The microstructural evolution is illustrated colour plots of x_M - ϕx_S, such as in the right hand side of Figure 2, which are scaled to the interval [0 1] in such a way that values lower/higher than the minimum/maximum value are converted to the minimum/maximum, respectively. Thus, the particle appears as a blue rectangle, the equilibrium metallic phase as red, the equilibrium oxidic phase as green and in the case of spinodal initialization, the initially supersaturated liquid appears as yellow.

4 Results and discussion

4.1 Qualitative comparison of the initialization methods

To illustrate the main differences between the initialization methods, a simplified morphology was chosen for the solid spinel particle: a rectangular particle of size [50 100 1]. Moreover, the wettability was chosen in between the low and high wettability regime, i.e. a contact angle of 90°, corresponding to an x_S-value of 0.74. The spinodal initialization was carried out for an initial supersaturation of x_i = 0.605 and for the random initialization, a volume fraction of 0.20 was proposed. Colour plots of x_M - ϕx_S of several time steps in the simulation with spinodal initialization are shown in Figure 4.

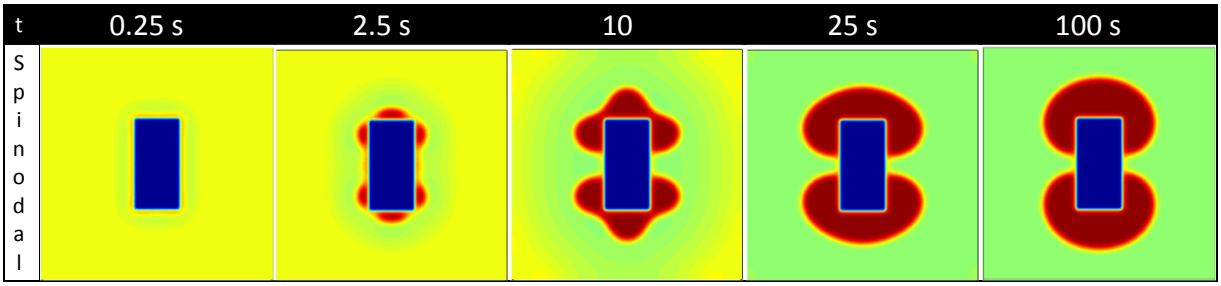

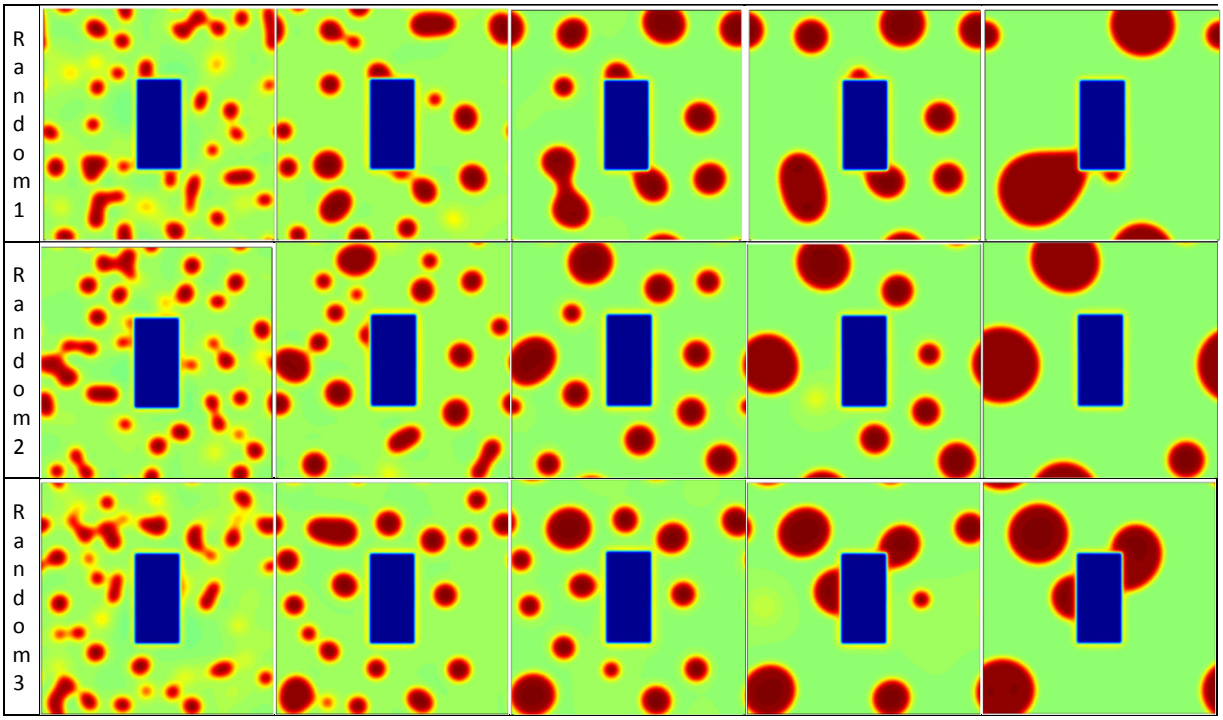

FIGURE 4 COLOUR PLOTS OF x_M - Φ x_S AFTER SEVERAL TIME STEPS IN THE SIMULATION IN A SYSTEM OF SIZE [256 256 1] AND WITH A SOLID PARTICLE OF SIZE [50 100 1] x_s=0.74; FIRST ROW: SPINODAL INITIALIZATION WITH x_i=0.605; SECOND ROW: RANDOM INITIALIZATION WITH f_V=0.20; THIRD ROW: SECOND SIMULATION OF RANDOM INITIALIZATION WITH f_V=0.20; FOURTH ROW: THIRD SIMULATION OF RANDOM INITIALIZATION WITH f_V=0.20

As was briefly mentioned in our previous work [8], first, 'localized' spinodal decomposition takes place around the solid particle. At low initial supersaturations, all metal is attached to the solid particle and thus the result is the same for several repeated simulations using different seedings for the random noise. For large x_i values, this is no longer the case, but the metal droplets still originate first near the solid particle. Colour plots of x_M - ϕx_S of several time steps in the simulation with the random initialization are shown in the second row of Figure 4. It is immediately clear that, in the resulting microstructure of a simulation with random initialization, the metallic droplets are more scattered over the complete slag phase. The attachment, however, is less obvious: e.g. the third row of Figure 4 shows colour plots of a simulation that initially has a small droplet attached to the particle, but due to Ostwald ripening

of larger droplets which are not attached to the solid, the attached droplet disappears and in the end, no metal is attached to the solid, even though this is energetically favourable. Furthermore, a third possibility exists: first no metal is attached to the solid particle, but then medium-sized droplets get attached to the solid (because this is energetically favourable) and these droplets grow by Ostwald ripening. This is illustrated in the bottom row of Figure 4. Thus it is immediately clear that the spread on the results for the random initialization will be far greater than for the spinodal initialization. For the random initialization, the droplets are positioned randomly over the entire system (except for the points where solid particles or other droplets are present). This may result in fewer attached droplets. E.g. it is possible that all larger droplets are concentrated in the border of the system, although the droplets are initialized on random positions. In such a case, the smaller droplets, situated around the particle, will dissolve and no droplets are attached to the particle, even though this might be favoured by the interfacial energies. Why such a situation occurs frequently in the simulations can be explained by considering Figure 5. It shows a system with size *[N N 1]* and a hatched particle with size *[Y X 1]*. The edge of the blue area is at an equal distance between the edges of the system and those of the solid particle.

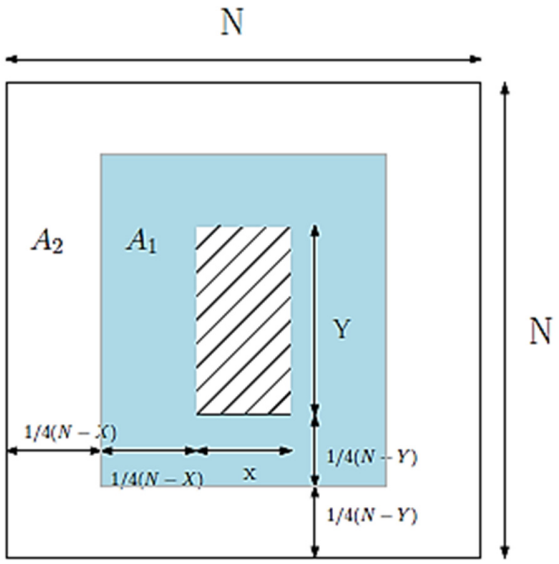

FIGURE 5 ILLUSTRATION OF THE AREAS UNDER CONSIDERATION IN THE RANDOM INITIALIZATION

The chance that a droplet is placed within a certain rectangle closer to or further away from the particle is determined by the amount of available positions within these rectangles. The area of the blue rectangle is

$$A_1 = \left(X + \frac{1}{2}(N - X)\right)\left(Y + \frac{1}{2}(N - Y)\right) - XY \quad \textbf{(4)}$$

And the total area available for droplets is $A_{tot} = N^2 - XY$. Thus the chance that a droplet is placed within the rectangle closer to the particle is

$$\frac{A_1}{A_{tot}} = \frac{1}{4}\frac{N^2 + N(X+Y) - 3XY}{N^2 - XY} \quad \textbf{(5)}$$

For the values in this work (*N*=256, *X*=50 and *Y*=100), this fraction is 0.367 and thus it is more likely that the droplets will be positioned further away from the solid particle. However, when real slag-spinel micrographs are used, the solid particles are usually more evenly distributed throughout the system and thus the effect of the position of the solid particles on the distribution of the randomly positioned metal droplets will be reduced.

4.2 Quantitative comparison of initialization methods

The spread on the results of simulations initialized with the spinodal decomposition method was determined based on three simulations with x_i = 0.605; x_S = 0.74 (the contact angle of the metal droplet on the solid particle is predicted to be θ = 90° and lies in between the low and high wettability regimes) in a system with size [256 256 1] with a rectangular particle of size [50 100 1]. The spread on the results of simulations with random initialization was determined based on five simulations with f_V = 0.20; x_S = 0.74 in a system with size [256 256 1] and a rectangular particle with size [50 100 1]. As noted previously, when real slag-spinel micrographs are used, the solid particles are usually more evenly distributed throughout the system and thus the effect of the position of the solid particles on the distribution of the randomly positioned metal droplets will be reduced. The values, averages and standard deviations of the results of these simulations can be found in the first two columns in Table 3.

	Spinodal decomposition **x_S = 0.74 ; x_i = 0.605**	***Random positioning*** **x_S = 0.74 ; f_V = 0.20**	***Spinodal decomposition*** **x_S = 0.60 ; x_i = 0.63**
Fraction metallic phase in the system	0.21311	0.18723	0.26348
	0.21296	0.18688	0.263777
	0.21306	0.18539	0.262967
	-	0.18939	0.263001
	-	0.18690	-
Average ± stdev	0.213 ± 7.64 10^{-5}	0.187 ± 0.00144	0.263 ± 0.0004
Fraction of metal attached to solid	1	0.57208	0.497492
	1	0	0.406688
	1	0	0.445757
	-	0.34331	0.513159
	-	0.33357	-
Average ± stdev	1 ± 0.0	0.250 ± 0.247	0.466 ± 0.042

TABLE 3 VALUES, AVERAGES AND STANDARD DEVIATIONS IN THE FRACTION METALLIC PHASE IN THE SYSTEM AND FRACTION METAL ATTACHED TO THE SOLID PARTICLES, FOR THE RESULTS OF BOTH INITIALIZATION METHODS AT THE LAST TIME STEP OF SEVERAL SIMULATIONS

Standard deviations for the fraction metallic phase in the system were generally three orders of magnitude smaller than the average value for random initialization and five orders of

magnitude for spinodal initialization. There is a larger spread on the fraction of metal present in the system for the random initialization because the initial volume fraction of metal was never exactly equal to 0.20. Metallic droplets are namely placed within the system as long as the actual volume fraction of metal does not exceed the prescribed value. The difference between both values can range from very small to large, as it is for example possible that the actual volume fraction only differs slightly from the prescribed value and that the last added droplet is quite large. Thus, in most cases, the actual volume fraction of metal after initialization (i.e. at the end of time step zero) will be larger than the intended value. However, in one case, the 20 trials for checking the overlap of the new droplet with the solid particles and the already present droplets in the system, did not suffice and the initialization was aborted. Then, the volume fraction of metal droplets was considerably smaller (0.1784) than the intended 0.20. One such exceedance was observed for micrograph 2 for the no wetting case (x_S = 0.50). This single simulation was repeated and the result of the second simulation are presented in this paper. The average value of the fraction of metal in the system given in Table 3 is smaller than the prescribed value, because the metal droplets are initialized with an x_M value of 0.50, but with sharp interfaces within a slag matrix with an x_M value of 0.98. The interfaces will become diffuse after time step zero and thus some of the metal that first belonged to a droplet will dissolve into the slag phase to form the diffuse interfaces. Hence, lowering the fraction of metallic droplets in the system.

For the fraction attached metal, the standard deviation is of the same order of magnitude as the average value for random initialization. For spinodal initialization, the standard deviation appeared to be zero for this case with an x_S value of 0.74 (in between the low and high

wettability regime, characterized with a contact angle of 90°), because all the metal present in the system was attached to the solid in all three simulations, i.e. a fraction of one for every simulation, as shown in Table 3. Previous work [8], however, showed that in general a certain spread is also present on the fraction of attached metal for spinodal initialization: simulations for x_i = 0.63; x_S = 0.60 were performed four times in a system with size [256 256 1] and a rectangular particle dimensions [50 100 1]. These results are shown in the last column of Table 3. This shows that the standard deviation for the fraction attached metal is at least one order of magnitude smaller than the average value.

Generally, the spinodal initialization method has a smaller spread on the results than the method with random positioning of metal droplets. The smaller spread on the amount of attached metal for the spinodal initialization can be explained by the fact that in the case of spinodal decomposition, the droplets are formed next to the solid particle and thus will be more easily attached to the solid if this is energetically favoured by the interfacial energy values. Moreover, as was explained above, with the random initialization , it is possible that all larger droplets are concentrated in the border of the system, resulting in the dissolution of the smaller droplets, situated around the particle, leaving no metal attached to the particle, even though this might be favoured by the interfacial energies: e.g. simulations 2 and 3 in Table 3.

4.3 Simulations with realistic spinel microstructures

Two initialization methods were compared to investigate which corresponds best to the real mechanism behind the interaction between the solid particles and liquid metal. The spinodal initialization would correspond in practice to some sort of reaction, whereas the random initialization corresponds more to the situation when the droplets and particles are formed

separately and then mixed in the slag. Realistic microstructures based on actual micrographs were used for the solid particles.

The spinodal initialization was carried out for an initial supersaturation of x_i = 0.605, which corresponds to a volume fraction of metal of 0.219. For the random initialization, the actual initial metal fraction is 0.196 ± 0.012 for x_S = 0.50 and 0.2015 ± 0.0009 for x_S = 0.58 for a proposed volume fraction of 0.20. Both initialization methods were applied for a non-wetting situation (x_S = 0.50) and an extremely low wetting case (x_S = 0.58 is the limit between the low and no wettability regimes). The results are shown as colour plots at different time steps throughout the simulation in Figure 6 and Figure 7.

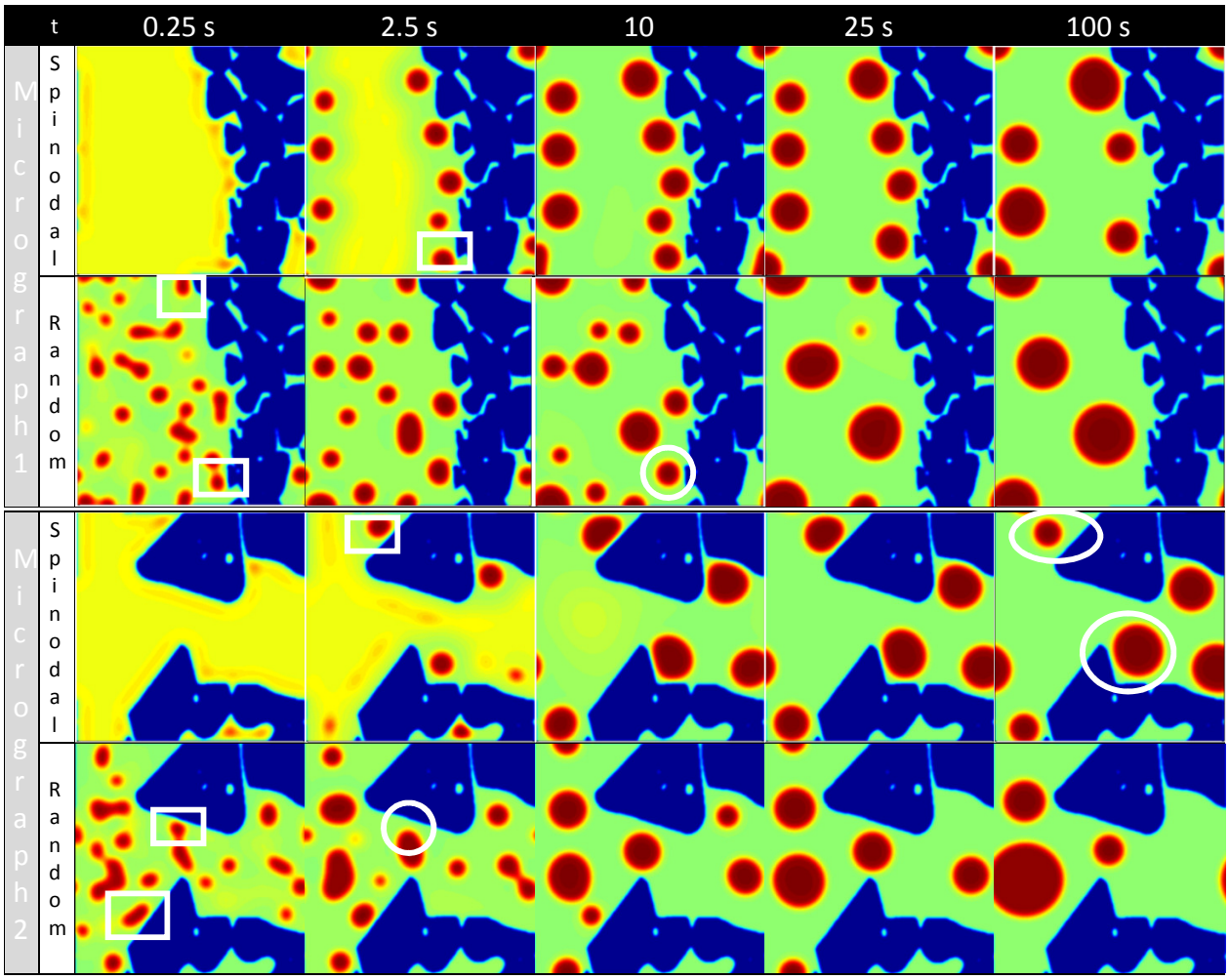

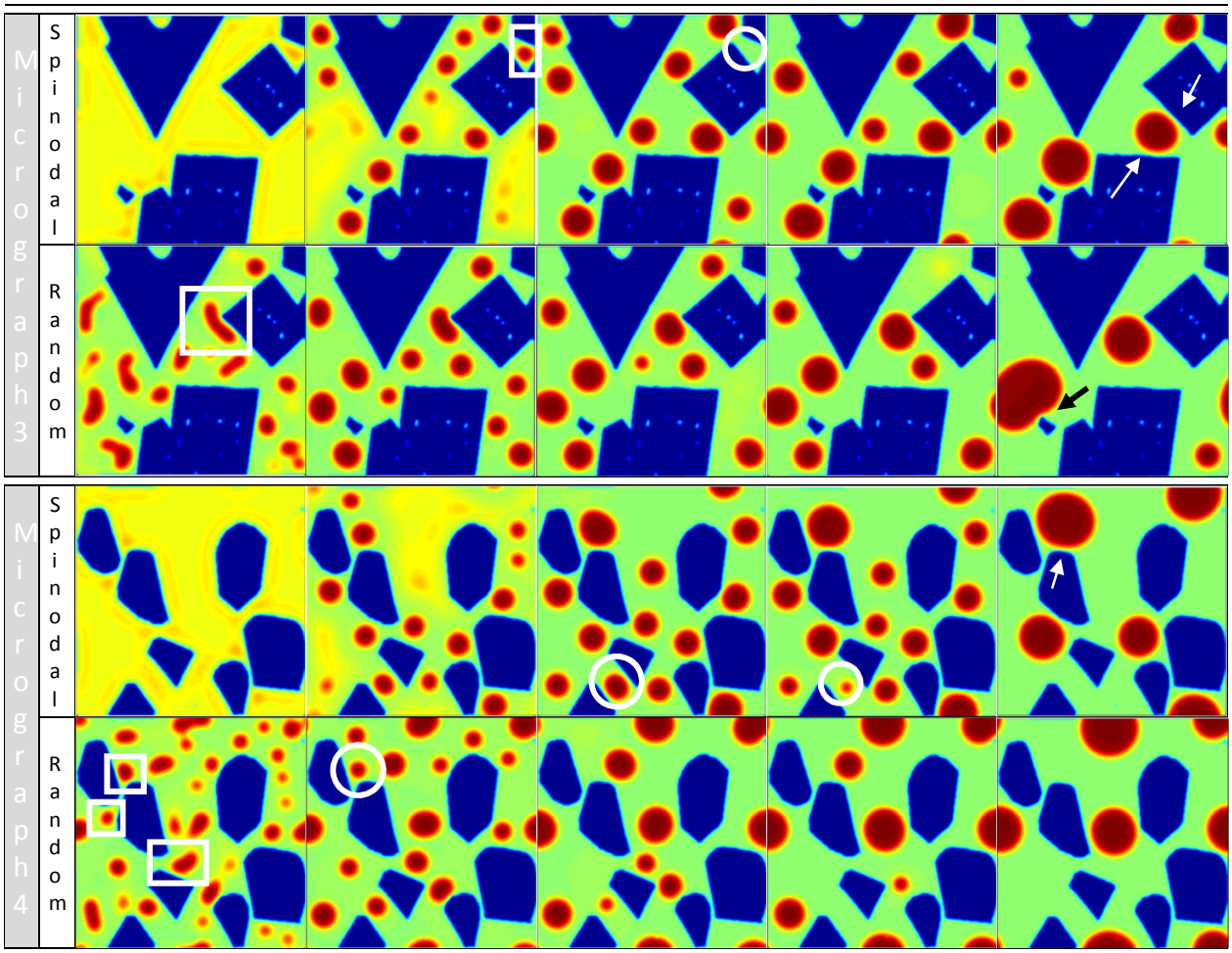

FIGURE 6 COMPARISON OF THE SPINODAL (UPPER ROW) AND RANDOM (LOWER ROW) INITIALIZATION METHODS IN A NON-WETTING SITUATION (x_S = 0.50)

In the case of spinodal decomposition, some metal is attached to solid particles in the first time steps, as indicated by the rectangles. Then this metal detaches or sometimes dissolves (marked by the circles). Depending on the shape of the particles, or more precisely, the amount of space available around the solid particles, some droplets are attached to solid particles again at intermediate time steps, as pointed to by the white arrows.

In the random initialization, some droplets are immediately attached to the solid particles (designated by the rectangles), but detached or dissolved again after approximately 10 s (indicated by the circles). In one simulation, one droplet was still attached to the solid at the

final time step of 100 s. This was, however, a very large droplet attached to a very small solid particle, as illustrated by the black arrow.

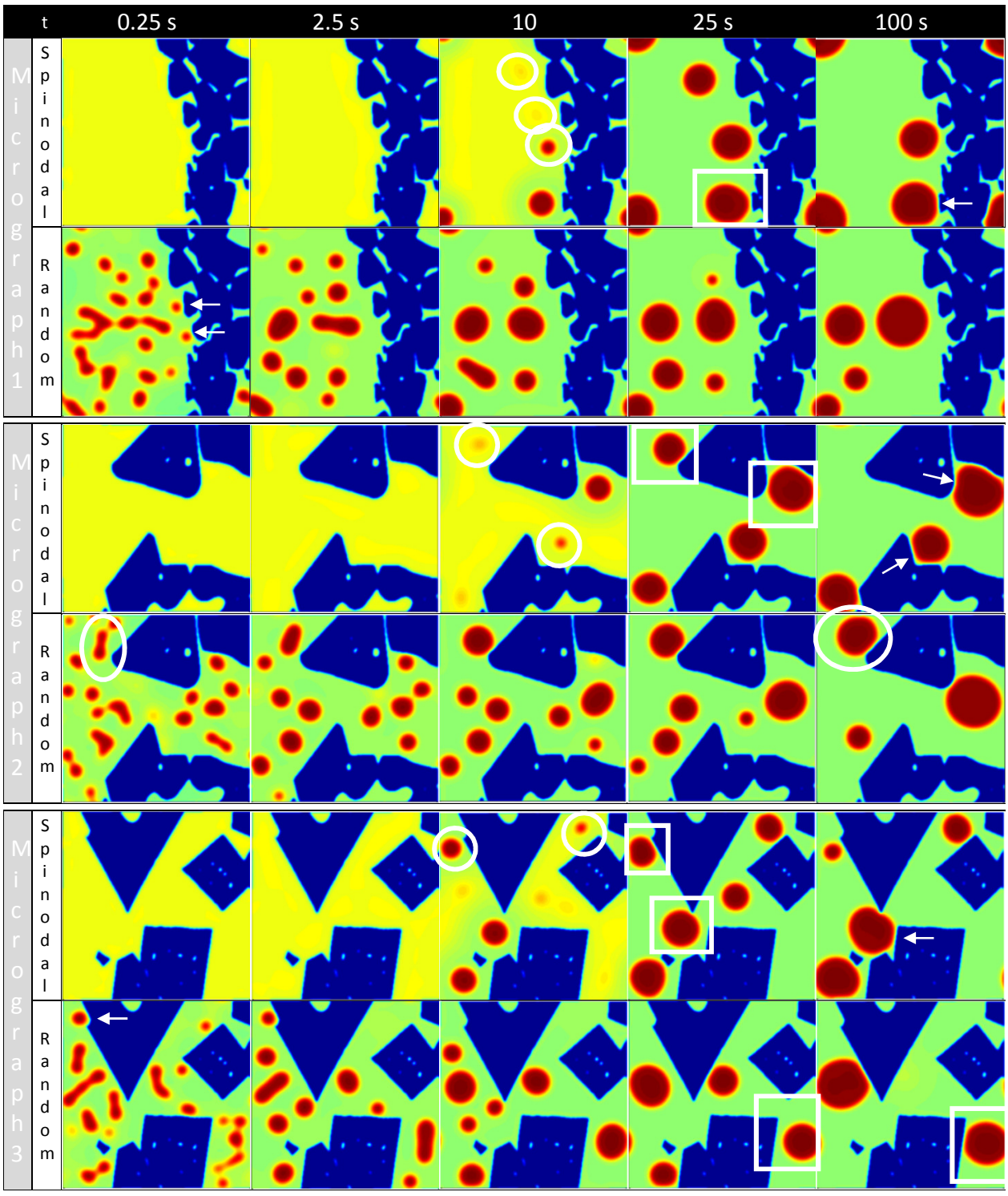

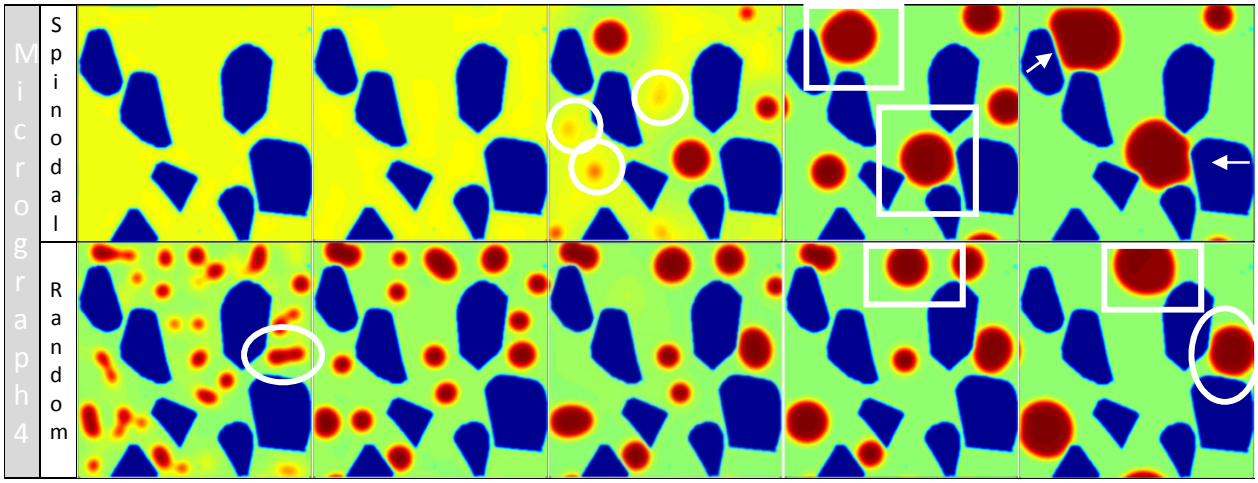

FIGURE 7 COMPARISON OF THE SPINODAL (UPPER ROW) AND RANDOM (LOWER ROW) INITIALIZATION METHODS IN AN EXTREME LOW WETTING SITUATION (x_s = 0.58)

For the spinodal initialization in the extreme low wetting case, the droplets initiate next to the solid particle (indicated by the circles) and grow subsequently to 'touch' the particle (marked by the rectangles). The droplets remain attached to the particles and even adopt their shape to the surrounding particles, as pointed to by the white arrows.

For the random initialization, three possibilities exist: the droplets are attached from the start to the end to the solid particles (indicated by the circles), the droplets are 'drawn' towards the solid particle and stay there until the end of the simulation (marked by the rectangles) or the attached droplets detach/dissolve immediately and no more droplets are attached afterwards (illustrated by the white arrows). The droplet needs to be initialized close enough to the particle and should be large enough to remain attached to the solid. If the droplet is not large enough, it will dissolve, even though it was initially attached to the particle. Larger droplets, when positioned nearby the solid, will move towards it in the case of low wettability.

Not only does spinodal decomposition provide a convenient way to introduce the metallic droplets in the system, it appears that in both wetting regimes, the spinodal decomposition corresponds best with the experimentally obtained microstructures (Figure 1), e.g. the

adaptation of the shape of the droplets to that of the solids in the simulations of the low wettability case (Figure 7). Moreover, it was observed experimentally that the attachment of the droplets is a non-equilibrium phenomenon [21]. This indicates that the droplets may originate through reaction with the solid particles, but that afterwards (once the reactions is finished), the droplets detach again. What corresponds with the observations for the simulations with spinodal decomposition in the non-wetting case.

It should be noted, however, that for the random initialization, attachment of droplets is also observed. This is mostly observed for the low wettability case and generally to a lesser extent than for the spinodal initialization. The fraction attached metal as a function of the particle fraction (characteristic for each micrograph) is shown in Figure 8.

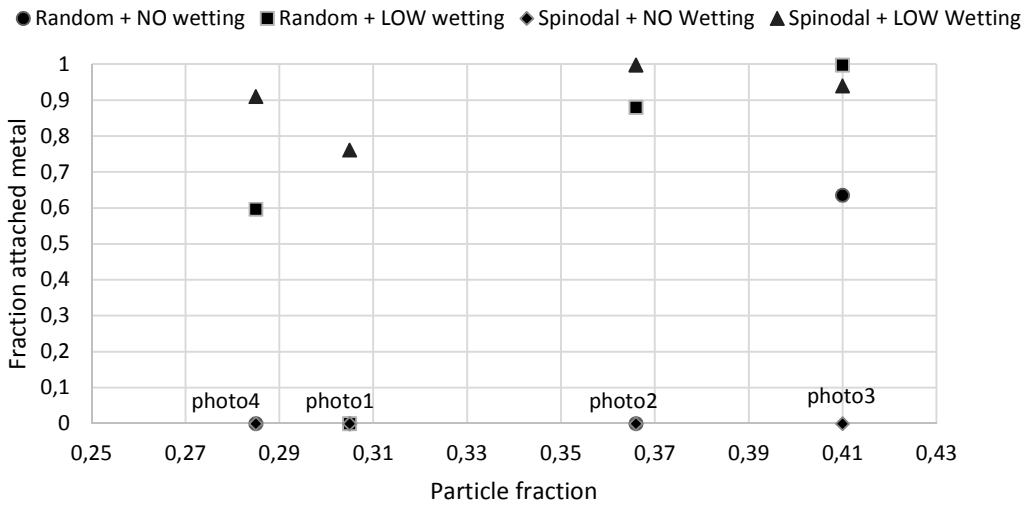

Figure 8 The fraction attached metal as a function of the particle fraction (characteristic for each micrograph, which is indicated by the label above the x-axis)

This shows that when the attachment is energetically favourable (in the low wettability regime), both initialization methods yield attached metal droplets. The 'no' wettability case, only provided attached metal droplets for micrograph 3 with the random initialization, as indicated by the black arrow in Figure 6. Micrograph number 1 (i.e. the upper left micrograph in

Figure 3 with solid particles mainly on the right side of the micrograph) with the random initialization did not yield any attached droplets in both wetting regimes, because the droplets were not initialized close enough to the particles. The random initialization would correspond to mixing separately formed metal droplets and solid particles and it would require in practice intensive mixing to make them collide.

The spinodal initialization yields attached droplets in both the no and the low wettability regime in the initial stages, but the droplets in the low wettability case stay attached to the solids. The droplets in the non-wetting case, however, remain in the close proximity of the particles.

5 Final discussion and conclusion

This study investigated the attachment of liquid droplets to solid particles in liquid slags with a phase field model [8,9], which was extended to consider realistic microstructures based on actual micrographs of the solid particles. In this model, the particles do not react with the liquid. The origin of the attachment was investigated by comparing two initialization methods for the metal droplets: by spinodal decomposition of a supersaturated liquid and a method with random positioning of the droplets. The first corresponds to a practical situation where the droplets are formed by a reaction nearby (and possibly together with) the spinel particles, whereas the latter corresponds to the situation where the droplets and particles are formed separately and then mixed randomly in the slag. Based on previous research, both methods were considered for two wettability regimes that seem to correspond best to the experimental system: no and low wettability.

From a simulation point of view, the random initialization poses no restrictions on the metal fraction of the system, as opposed to the spinodal decomposition, where the initial

supersaturation x_i should be selected in between the inflection points of the free energy curve representing the spinodal. The random initialization, however, leads to a much larger spread on the results than the spinodal initialization. As a consequence, a larger number of simulations are required to draw relevant conclusions for the random initialization than when the droplets form through spinodal decomposition of a supersaturated slag, since the droplets are then first formed close to the particle.

Previous results [9] indicated the correspondence of the experimental PbO-FeO-CaO-SiO_2-Cu_2O-ZnO-Al_2O_3 system [1] to the low wettability regime in the model under consideration. These were confirmed, because the attachment was more pronounced in the low wettability case and the droplets adapted their shape to the surrounding solids, as is also observed in experiments [21]. Moreover, experimentally, the actual 'attachment' of the droplets seems to be a non-equilibrium phenomenon, which is in correspondence with the results for the spinodal initialization, as in that case the droplets are first attached to the solid due to the originating reaction and are afterwards also detached/dissolved (when waiting long enough).

The similar behaviour between simulated microstructures obtained with the spinodal initialization with experimental micrographs shows that the droplet-particle interaction could originate from a chemical interaction in which the droplet and the particle are involved. This hypothesis was also confirmed by recent experimental findings of De Wilde et al. [21] in a PbO-FeO-CaO-SiO_2-Cu_2O-ZnO-Al_2O_3 system. These show the growth of solid spinel particles on the edge of already existing metallic droplets or their formation together with new droplets. They also proposed a mechanism for this observation: the spinel solids and copper droplets form together due to a simultaneous reduction of copper oxides into metallic copper and the

oxidation of slag oxides into more stable spinel structures. Additionally, the spinel solids can also form on an already present Cu droplet in an analogous way.

The non-reactive random interaction is based only on differences in interfacial energies. But it became apparent that even though the attachment is energetically favourable in the low wettability case, it will not necessarily take place because a certain barrier needs to be overcome. In practice, overcoming this barrier could be done by heavily mixing the solution containing the droplets and solids [21]. On the other hand, some metal attachment could be observed in the non-wetting case, but this seemed to be coincidental.

In the non-wetting case, the spinodal initialization gave the microstructures in best correspondence with the experiments, but in the low wettability case, the simulation results of both initialization methods correspond well with the experimental system. This confirms that the droplet-particle interaction can have multiple origins: either reactive or non-reactive, as implied by De Wilde et al. [21].

It is still unclear which of the two possible origins lays at the base of the attachment. Therefore, more simulations and experiments focussing on the two origins, will be executed in the future. As models including convection already exist, explicit implementation of a model of the formation of the solid particles within a liquid slag together with or on the side of a liquid metal droplet in a multicomponent multiphase system will allow us to simulate and study the reactive origin for the attachment in more detail.

6 Acknowledgments

I. Bellemans holds a PhD fellowship of the Research Foundation - Flanders (FWO). The authors also acknowledge the work done by J. Van De Sande in the frame of his bachelor thesis.

References

[1] E. De Wilde, I. Bellemans, M. Campforts, A. Khaliq, K. Vanmeensel, D. Seveno, M. Guo, A. Rhamdhani, G. Brooks, B. Blanpain, N. Moelans, K. Verbeken, Mater. Sci. Technol. 31 (2015) 1925–1933.
[2] R. Sridhar, J.M. Toguri, S. Simeonov, Metall. Mater. Trans. B 28 (1997) 191–200.
[3] J. Yannopoulos, Can. Metall. Q. 10 (1970) 291–307.
[4] F.A. Calvo, A. Ballester, Metall. Trans. B 17 (1986) 267–270.
[5] M.A. Nkohla, Characterization of Ferrochrome Smelter Slag and Its Implications in Metal Accounting, Cape Peninsula University of Technology, 2006.
[6] E. De Wilde, I. Bellemans, S. Vervynckt, M. Campforts, K. Vanmeensel, N. Moelans, K. Verbeken, Proc. EMC 2013 1 (2013) 161–174.
[7] E. De Wilde, I. Bellemans, M. Campforts, M. Guo, K. Vanmeensel, B. Blanpain, N. Moelans, K. Verbeken, in:, Proc. EMC 2015, Düsseldorf, Germany, 2015.
[8] I. Bellemans, N. Moelans, K. Verbeken, Comput. Mater. Sci. 108, Part B (2015) 348–357.
[9] I. Bellemans, E. De Wilde, N. Moelans, K. Verbeken, Acta Mater. 101 (2015) 172–180.
[10] N. Moelans, B. Blanpain, P. Wollants, Calphad 32 (2008) 268–294.
[11] S.Y. Hu, J. Murray, H. Weiland, Z.K. Liu, L.Q. Chen, Calphad 31 (2007) 303–312.
[12] J. Heulens, B. Blanpain, N. Moelans, Acta Mater. 59 (2011) 2156–2165.
[13] S.M. Allen, J.W. Cahn, Acta Metall. 27 (1979) 1085–1095.
[14] T. Sakai, S.W. Ip, J.M. Toguri, Metall. Mater. Trans. B 28 (1997) 401–407.
[15] H. Sun, K. Nakashima, K. Mori, ISIJ Int. 46 (2006) 407–412.
[16] N. Moelans, Acta Mater. 59 (2011) 1077–1086.
[17] L.-Q. Chen, J. Shen, Comput. Phys. Commun. (1998) 147–158.
[18] Matlab 7.12.0 (R2011a), The MathWorks Inc., Natick, MA, 2011.
[19] S. Mostafaee, M. Andersson, P. Jönsson, Ironmak. Steelmak. 37 (2010) 425–436.
[20] J.W. Cahn, Acta Metall. 9 (1961) 795–801.
[21] E. De Wilde, I. Bellemans, L. Zheng, M. Campforts, M. Guo, B. Blanpain, N. Moelans, K. Verbeken, Mater. Sci. Technol. (accepted).